Science and Technology Indonesia
e-ISSN:2580-4391 *p*-ISSN:2580-4405
Vol. 7, No. 1, January 2022

Research Paper

Synthesis and Characterization of Fe-Doped $CaTiO_3$ Polyhedra Prepared by Molten NaCl Salt

Dwi Rahayu Novianti[1], Fikri Haikal[1], Usman Ali Rouf[1], Arie Hardian[2], Anton Prasetyo[1]*

[1]*Department of Chemistry, Faculty of Science and Technology, Universitas Islam Negeri Maulana Malik Ibrahim Malang, Malang, 65144, Indonesia*
[2]*Department of Chemistry, Faculty of Sciences and Informatics, Universitas Jenderal Achmad Yani, Cimahi, 40531, Indonesia*
***Corresponding author**: anton@kim.uin-malang.ac.id

Abstract
$CaTiO_3$ as one of the perovskite-based photocatalysts has a band gap energy of 3.5 eV (~354 nm), thus will work at the ultraviolet light region. One of the strategies to decrease the band gap energy is doping metal. In this research, $CaTiO_3$ was doped by Fe element as purposes to decreasing its band gap energy. Fe doped $CaTiO_3$ with different Fe concentrations (0, 5, 10, 15, and 20%) compounds were synthesized using molten NaCl salt method. The diffractogram samples showed that the Fe-doped $CaTiO_3$ crystal was successfully prepared. The refinement results showed that the samples have space group Pbnm a with R_p and R_{wp} values below 12%. The SEM images showed that the particle shape was regular polyhedra morphology, and doping Fe^{3+} caused the particle size to decrease and agglomerate. The UV-Vis DRS spectra showed that the Fe-dopant revealed the absorption light at visible range wavelength by meaning that Fe-dopant successfully lowered the band gap value of CTO (3.43 eV)

Keywords
Fe-doped $CaTiO_3$, Molten NaCl Salt, Photocatalyst

Received: 20 August 2021, Accepted: 23 November 2021
https://doi.org/10.26554/sti.2022.7.1.17-21

1. INTRODUCTION

It is well known that perovskite structure (ABO_3) has good potential to be applied as a photocatalyst material (Wang et al., 2021; Wei et al., 2021). $CaTiO_3$ is one of the perovskite structure class materials that can be used as a photocatalyst with band gap energy of 3.5 eV and relatively low rate recombination (Jang et al., 2011). The high band gap energy of $CaTiO_3$ makes it less efficient because it just work in the ultraviolet region (UV). Therefore, it is certainly not beneficial for the application of $CaTiO_3$ as a photocatalyst material. Many researchers have been reported that aliovalent metal doping in perovskite structure compound can reduces the band gap energy value (Huang et al., 2016; Jang et al., 2011; Lozano-Sanchez et al., 2015; Passi and Pal, 2021; Kumar et al., 2020; Zhang et al., 2018). Perovskite structure compound has a unique structure, where A or B cation can be substituted with other cations to obtain more attractive characteristics. The substitution of A or B cation will change the composition and symmetrical structure of perovskite material and form cation or anion vacancies that affect the band gap energy and photocatalytic activity. Thus, doping at A or B-site cation is one of the best ways to improve the photocatalytic property of $CaTiO_3$ material (Wang et al., 2015). In addition, tuning morphology particle of photocatalyst is also other strategies to enhance the photocatalytic activity (Cheng et al., 2021; Zhou et al., 2020).

Some metals have been reported as a dopant for $CaTiO_3$ material, such as Zr (Huang et al., 2016), Er (Lozano-Sanchez et al., 2015), Fe (Jang et al., 2011), and Mn (Zhang et al., 2018). Meanwhile, Yang et al. (2014) had successfully synthesized the Fe-doped $CaTiO_3$ material using the solid-state reaction method and reported that Fe could increase the photocatalytic activity of $CaTiO_3$. It also was reported that Fe dopant revealed the new transition electronic between the valence band and the conduction band of $CaTiO_3$, and caused revealing the light absorption in the visible region (Jang et al., 2011) and then improved the photocatalytic activity in methylene blue degradation (MB). Yang et al. (2014) also reported agglomeration in Fe-doped $CaTiO_3$ particle caused by high-temperature condition in the solid-state method synthesized (Markovic et al., 2008). Meanwhile, the agglomeration in material influences the optical properties and decreases the photocatalytic activity (Pellegrino et al., 2017). Therefore, the Fe-doped $CaTiO_3$ material without agglomeration particle formed is needed to improve its photocatalytic activity. In addition, the $CaTiO_3$ morphology particle has also been reported to influence the photocatalytic activity (Yoshida et al., 2015; Zhuang et al.,

2014).

Molten salt synthesis (MSS) is a simple and green method commonly used to synthesize high-purity of metal oxide with composition and morphology tuning and decreases the agglomeration (Gupta and Mao, 2021; Kimura, 2011). The synthesis of $CaTiO_3$ using MSS was reported by many researchers and found a unique morphology. Yoshida et al. (2015) synthesized $CaTiO_3$ using NaCl molten salt and obtained the regular polyhedra morphology with high photocatalytic activity. On other hand, tuning morphology of Fe doped photocatalyst material have reported others researcher. Liu et al. (2017) have been successfully synthesized nanosheets Fe doped $Bi_4Ti_4O_{12}$ using MSS which reported having high activity photocatalytic. It's indicates that morphology tuning in Fe doped $CaTiO_3$ can be used as a technique to increase its photocatalytic activity. In this research, we prepared Fe-doped $CaTiO_3$ with different Fe concentrations from 0 to 20% with step size 5% using the molten NaCl salt method. The samples were characterized using the X-Ray diffraction (XRD) technique, scanning electron microscopy-energy dispersive X-ray spectroscopy (SEM-EDS), and ultraviolet-visible diffuse reflectance spectroscopy (UV-Vis DRS).

2. EXPERIMENTAL SECTION

2.1 Materials

Chemicals and materials: $CaCO_3$ (Merck, powder 99.9%), TiO_2 (Sigma-Aldrich, powder 99.9%), Fe_2O_3 (Sigma-Aldrich, powder 99.9%), NaCl (Merck, powder 99.5%), acetone (Merck, p.a).

2.2 Synthesis

In this study, we prepared $CaTiO_3$ (CTO), $CaTi_{0.95}Fe_{0.05}O_3$ (CTOF0.05), $CaTi_{0.90}Fe_{0.10}O_3$ (CTOF0.10), $CaTi_{0.85}Fe_{0.15}O_3$ (CTOF0.10), $CaTi_{0.85}Fe_{0.15}O_3$ (CTOF0.15), and $CaTi_{0.80}Fe_{0.2}O_3$ (CTOF0.2). The requirement precursors depend on stoichiometric calculation. The precursors are weighed, and ground to a fine powder using an agate mortar and pestle for 1 hour. Sometimes, acetone is used as a mixing medium to get a homogeneous mixture (Zuniga et al., 2018). Then, all samples were calcined at 700^{o}C for 6 hours. The powders were then mixed with NaCl solid in the ratio of 1:7. All solid solutions were then calcined at 900^{o}C for 8 hours, followed by cooling down to room temperature and washing 3-5 times with hot water to remove the salt ions (Mao et al., 2007).

2.3 Characterization

The phase and crystal structure were analyzed from the X-ray diffraction patterns. All diffraction patterns were obtained by using Panalytical Xpert-pro (Panalytical, Almelo, Netherland) diffractometer measurement with Cu Kα (1.5406 Å) at range measurement 2θ (^{o}): 20-80. The lattice parameters were obtained from the refinement process using Le Bail method available in RIETICA software (Hunter , 2000). The morphologies and elemental compositions of the compounds were characterized using SEM-EDS type of JSM 6510 LA (JEOL, Tokyo, Japan). The absorption spectrum of all powders were obtained using Shimadzu UV-2450 spectrometer (Shimadzu, Kyoto, Japan) at the wavelength of 200-800 nm.

3. RESULTS AND DISCUSSION

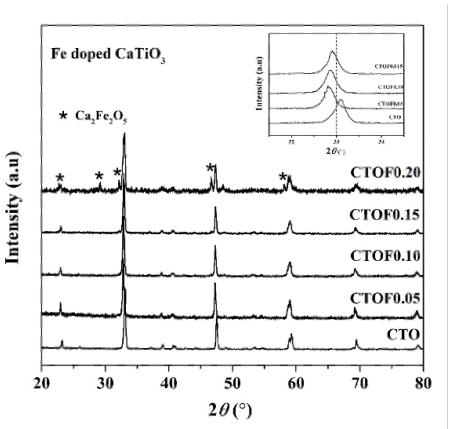

Figure 1. XRD Pattern of Fe-doped $CaTiO_3$ (Inset: Peak Shifting at 2θ (°): 32.96)

Figure 1 showed the diffractogram sample and matched it with standard data of $CaTiO_3$ in the Joint Committee on Powder Diffraction Standards (JCPDS) No.82-0229 and indicate that the target sample was successfully synthesized. The result also showed that the samples have a single-phase except for CTOF0.20. The typical peak found at 2θ (°): 29.15, 32.19, 46.61, and 58.13. However, the secondary phase in $CTOF_{0\cdot20}$ was $Ca_2Fe_2O_5$ identified from the diffraction peak at 2θ (°): 22.7, 29.2, 32.1, and 46.6 (JCPDS cards no. 89-8662).

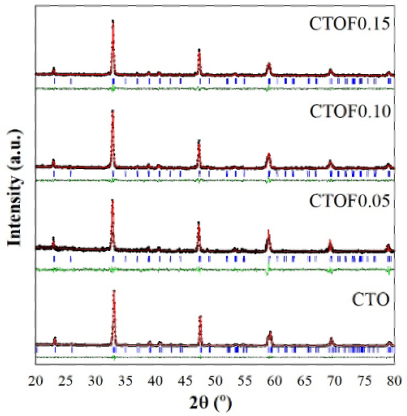

Figure 2. XRD Refinement Result for CTO and CTOF with Different Doping Concentration. (Black Dot Symbol (•) for Experimental Data, Red Lines (-) for Calculation Data, Blue Line (|) for The Peak Position, and Green Line (-) for The Difference Between Experimental Data and Calculation)

Table 1. Crystallographic Data of Fe-doped $CaTiO_3$

Parameters	Samples			
	CTO	CTOF0.05	CTOF0.1	CTOF0.15
Crystal system	Orthorhombic	Orthorhombic	Orthorhombic	Orthorhombic
Space group	Pbnm	Pbnm	Pbnm	Pbnm
a (Å)	5.3799(2)	5.4085(8)	5.3964(5)	5.3948(5)
b (Å)	5.4402(3)	5.406(1)	5.403(1)	5.409(1)
c (Å)	7.6423(4)	7.6168(8)	7.6334(9)	7.629(2)
V (Å^3)	223.68(2)	222.71(6)	222.57(6)	222.62(7)
R_p(%)	10.57	16.56	11.42	10.02
R_{wp}(%)	5.9	14.1	8.88	9.24
GoF(X^2)	0.035	0.041	0.062	0.12

The $Ca_2Fe_2O_5$ was a perovskite with oxygen vacancy and it is well-known as brownmillerite structure ($A_2B_2O_5$) (Silva and Sombra, 2011). The formed $Ca_2Fe_2O_5$ represents the maximum concentration of Fe dopant to replace Ti in $CaTiO_3$ structure without changing the original structure (Jang et al., 2011). All refined diffractograms, except $CTOF_{0\cdot20}$, were depicted in Figure 2 and all parameters were summarized in Table 1.

Based on Figure 2 and Table 1, the refinement result can be accepted (Toby, 2006). The result showed that the CTOF materials have been successfully prepared with orthorhombic crystal and Pbnm space group. Inset in Figure 1 represents the Fe^{3+} dopant caused the peak at 2θ (°): 32.96 shifted. It was reported that the main peak was shifted to the lower 2θ, indicating the crystal lattice has changed. This result relates to the difference in the ionic crystal radii of Ti^{4+} (0.605 Å) and Fe^{3+} (0.645 Å) which caused a change in the crystal lattice of the CTO structure (Xia et al., 2018). This result showed that Fe ion successfully replaces Ti ion, partially.

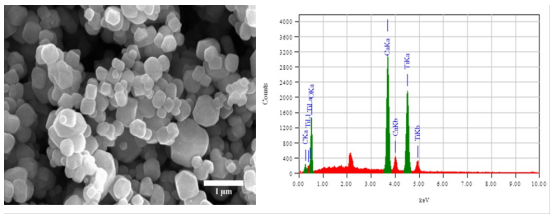

Figure 3. SEM Image, and EDS Spectrum of CTO

The SEM images and EDS spectrum of all samples were depicted in Figure 3 and 4. As it can be seen that the particle has polyhedra morphology. Many researchers reported various morphologies of CTO such as spheric, walnut-like, cubic, sphere, plate-like, and whisker, which were synthesized by different methods and parameters (Zhao et al., 2013; Karthikeyan et al., 2020; Yoshida et al., 2014; Saito et al., 2008; Zhang et al., 2013). These morphologies indicate that parameters and methods in synthesis influence the morphology of particles. The polyhedra morphology of CTO was similar to a previous report by Yoshida et al. (2014), whom synthesized CTO using the molten NaCl salt method. They were also reported that synthesis using different salt flux lead to different morphology. Based on Figure 4, the particle sizes were decreasing but they agglomerated. It indicates that Fe doping influences the growth of CTO grain particles (Huang et al., 2016; Luo et al., 2021). Sato et al. (2019) reported that the substitution of Ti^{4+} with Fe^{3+} with a smaller charge caused an unbalance charge, thus compensated by the reveal of oxygen vacancy. This vacancy detains the ion movement cause decreasing the grain growth and particle size.

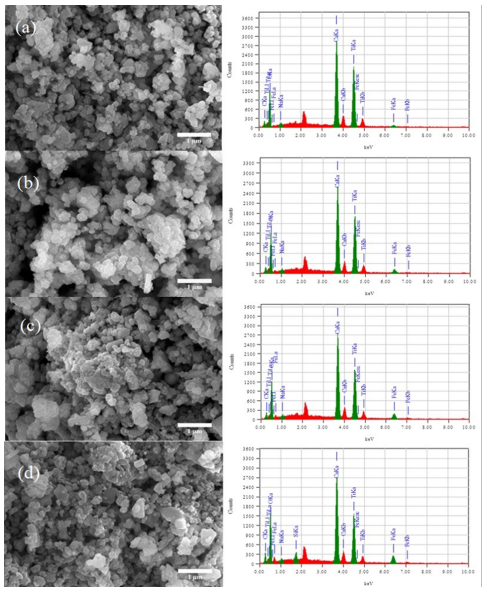

Figure 4. SEM Images, and EDS Spectra of (a) CTOF0.05, (b) CTOF0.10, (c) CTOF0.15, and (d) CTOF0.2

The EDS result exhibiting the elemental composition of Fe-doped CTO were summarized in Table 2. The result shows that Ca, Ti, Fe, and O were found and indicated that the constituents' elements matched. The percentage of Fe element increases, which corresponds to the mol concentration Fe dopant.

Table 2. The Elemental Composition of Fe-doped CTO

Samples	Ca (%)	Ti (%)	Fe (%)	O (%)
CTO	26.02	31.3	-	40.38
CTOF0.05	26.04	31.47	1.88	37.32
CTOF0.10	25.52	29.03	3.99	38.12
CTOF0.15	25.56	26.74	6.16	37.35
CTOF0.20	24.23	22.4	8.41	39.32

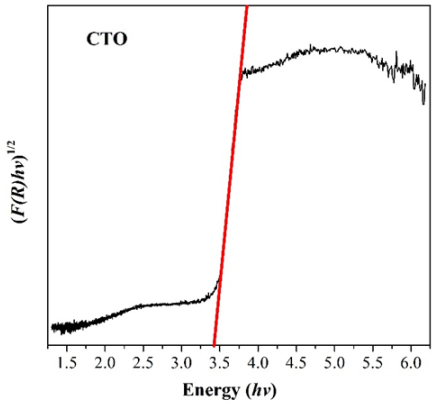

Figure 5. Tauc-Plot Spectrum DRS CTO

The band gap energy of the CTO was 3.43 eV (361 nm) which is obtained from the Tauc-plot method depicted in Figure 5. The light reflectance of CTOFs were shown in Figure 6, and it can be seen that there was a change in light reflectance character. The Fe dopant reveals decreases of reflectance and red-shifted. It indicated that the absorption light in the visible increases due to Fe^{3+} dopant. A similar phenomenon with the previous report by Jang et al. (2011) and Yang et al. (2014) that observes the Fe substitution to $CaTiO_3$ crystal lattice revealed the new energy band state between the conduction band and the valence band and having lower band gap energy than $CaTiO_3$ (Jang et al., 2011). It is also reported that the CTO band gap involved the electronic transition of O 2*p* orbitals (valence band) to Ti 3*d* orbitals (conduction band), while the Fe-doped CTO has emerged a new electronic transition with lower energy and carrying electron of Fe_{eg} to Fe 4*s* (Jang et al., 2011). Revealing light absorption in the visible region is important to increase its photocatalytic activity.

4. CONCLUSIONS

The CTO and Fe-doped CTO (CTOF) were successfully synthesized using the molten NaCl salt method and with space group Pbnm. Nevertheless, at 20% of Fe concentration, it formed secondary phase which is $Ca_2Fe_2O_5$. All obtained powders have regular polyhedra morphologies with the size inversely proportional with the Fe concentration. DRS spectra of samples showed that Fe dopant revealed the absorptions light at visible wavelength. These results suggested that MSS is

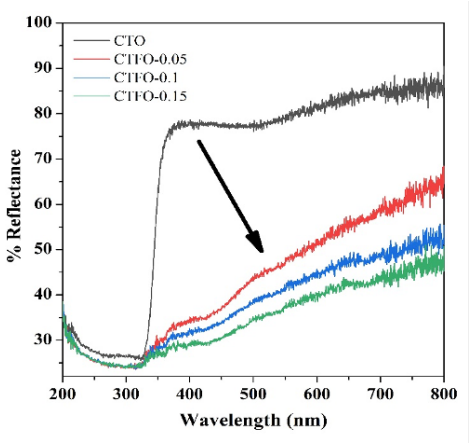

Figure 6. UV-Vis DRS Spectra of CTO, and CTOF Powders

potential to synthesize metal-doped photocatalyst with tuning morphology strategies.

5. ACKNOWLEDGEMENT

We want to thank all members of our research group for discussing the research results written in this manuscript.

REFERENCES

Cheng, T., X. Sun, T. Xian, Z. Yi, R. Li, X. Wang, and H. Yang (2021). Tert-Butylamine/Oleic Acid-Assisted Morphology Tailoring of Hierarchical $Bi_4Ti_3O_{12}$ Architectures and Their Application for Photodegradation of Simulated Dye Wastewater. *Optical Materials*, **112**; 110781

Gupta, S. K. and Y. Mao (2021). A Review on Molten Salt Synthesis of Metal Oxide Nanomaterials: Status, Opportunity, and Challenge. *Progress in Materials Science*, **117**; 100734

Huang, X. J., Y. Xin, H. Y. Wu, F. Ying, Y. H. Min, W. S. Li, S. Y. Wang, and Z. J. Wu (2016). Preparation of Zr-doped $CaTiO_3$ With Enhanced Charge Separation Efficiency And Photocatalytic Activity. *Transactions of Nonferrous Metals Society of China*, **26**(2); 464−471

Hunter, B.A. (2000). *Rietica- A Visual Rietveld Program.* Austalia: Australian Nuclear Science and Technology Organisation

Jang, J. S., P. H. Borse, J. S. Lee, K. Lim, O. Jung, E. D. Jeong, J. S. Bae, and H. G. Kim (2011). Photocatalytic Hydrogen Production In Water-Methanol Mixture Over Iron-Doped $CaTiO_3$. *Bulletin of The Korean Chemical Society*, **32**(1); 95−99

Karthikeyan, C., M. Thamima, and S. Karuppuchamy (2020). Structural and Photocatalytic Property of $CaTiO_3$ Nanosphere. In *Materials Science Forum*, **982**; 169−174

Kimura, T. (2011). *Molten Salt Synthesis of Ceramic Powders Advances in Ceramics Synthesis and Characterization Processing and Specific Applications*. Japan: Rijeka In Technology

Kumar, A., A. Kumar, and V. Krishnan (2020). Perovskite Ox-

ide Based Materials for Energy and Environment-Oriented Photocatalysis. *ACS Catalysis*, **10**(17); 10253–10315

Liu, Y., G. Zhu, J. Gao, M. Hojamberdiev, R. Zhu, X. Wei, Q. Guo, and P. Liu (2017). Enhanced Photocatalytic Activity of $Bi_4Ti_3O_{12}$ Nanosheets by Fe^{3+}-Doping and The Addition of Au Nanoparticles: Photodegradation of Phenol And Bisphenol A. *Applied Catalysis B: Environmental*, **200**; 72–82

Lozano-Sanchez, L., S. Obregon, L. Diaz-Torres, S. W. Lee, and V. Rodriguez-Gonzalez (2015). Visible And Near-Infrared Light-Driven Photocatalytic Activity of Erbium-Doped $CaTiO_3$ System. *Journal of Molecular Catalysis A: Chemical*, **410**; 19–25

Luo, L., S. Wang, H. Wang, C. Tian, and B. Jiang (2021). Molten-Salt Technology Application for the Synthesis of Photocatalytic Materials. *Energy Technology*, **9**(2); 2000945

Mao, C., G. Wang, X. Dong, Z. Zhou, and Y. Zhang (2007). Low Temperature Synthesis Of $Ba_{0.70}Sr_{0.30}TiO_3$ Powders By The Molten-Salt Method. *Materials Chemistry and Physics*, **106**(2-3); 164–167

Markovic, S., M. Mitric, G. Starcevic, and D. Uskokovic (2008). Ultrasonic De-Agglomeration of Barium Titanate Powder. *Ultrasonics Sonochemistry*, **15**(1); 16–20

Passi, M. and B. Pal (2021). A Review on $CaTiO_3$ Photocatalyst: Activity Enhancement Methods And Photocatalytic Applications. *Powder Technology*, **388**; 274-304

Pellegrino, F., L. Pellutie, F. Sordello, C. Minero, E. Ortel, V.-D. Hodoroaba, and V. Maurino (2017). Influence of Agglomeration and Aggregation on The Photocatalytic Activity of TiO_2 Nanoparticles. *Applied Catalysis B: Environmental*, **216**; 80–87

Saito, Y., H. Takao, and K. Wada (2008). Synthesis Of Plate-Like $CaTiO_3$ Particles by a Topochemical Microcrystal Conversion Method and Fabrication of Textured Microwave Dielectric Ceramics. *Ceramics International*, **34**(4); 745–751

Sato, N., M. Haruta, K. Sasagawa, J. Ohta, and O. Jongprateep (2019). Fe and Co-doped (Ba, Ca) TiO_3 Perovskite as Potential Electrocatalysts for Glutamate Sensing. *Engineering Journal*, **23**(6); 265–278

Silva, C. C. d. and A. S. Sombra (2011). Temperature Dependence of The Magnetic and Electric Properties of $Ca_2Fe_2O_5$. *Materials Sciences and Applications*, **2**; 1349-1353

Toby, B. H. (2006). R Factors in Rietveld Analysis: How Good Is Good enough *Powder Diffraction*, **21**(1); 67–70

Wang, H., Q. Zhang, M. Qiu, and B. Hu (2021). Synthesis and Application of Perovskite-based Photocatalysts in Environmental Remediation: A Review. *Journal of Molecular Liquids*, **334**; 116029

Wang, W., M. O. Tade, and Z. Shao (2015). Research Progress of Perovskite Materials in Photocatalysis and Photovoltaics Related Energy Conversion and Environmental Treatment. *Chemical Society Reviews*, **44**(15); 5371–5408

Wei, K., Yousef, F., Yao, G., Xie, R., and Lai, B. (2021). Strategies For Improving Perovskite Photocatalysts Reactivity For Organic Pollutants Degradation: A Review On Recent Progress. *Chemical Society Reviews*, **44**(15); 5371–5408

Xia, J., H. Li, H. You, Z. Wu, J. Chen, Z. Lu, L. Chen, M. Wang, and Y. Jia (2018). Effects of Fe Doping on Photoluminescent and Magnetic Properties of $CaTiO_3$: Eu^{3+}. *Ceramics International*, **44**(17); 21530–21532

Yang, H., C. Han, and X. Xue (2014). Photocatalytic Activity of Fe-doped $CaTiO_3$ Under UV–Visible Light. *Journal of Environmental Sciences*, **26**(7); 1489–1495

Yoshida, H., M. Takeuchi, M. Sato, L. Zhang, T. Teshima, and M. G. Chaskar (2014). Potassium Hexatitanate Photocatalysts Prepared by a Flux Method for Water Splitting. *Catalysis Today*, **232**; 158–164

Yoshida, H., L. Zhang, M. Sato, T. Morikawa, T. Kajino, T. Sekito, S. Matsumoto, and H. Hirata (2015). Calcium Titanate Photocatalyst Prepared by a Flux Method for Reduction of Carbon Dioxide with Water. *Catalysis Today*, **251**; 132–139

Zhang, Y., X. Nai, M. Wei., D. Zhu, C. Zhu, and W. Li (2013). Preparation and Characterization of Calcium Titanate ($CaTiO_3$) Whiskers Via Molten Salt Method. *In Advanced Materials Research*, **630**; 89–92

Zhang, Z., Huihong Lu, H., Li, X., Li, X., Ran, S., Chen, Z., Yang, Y., Wu, X., and Li, L. (2019). Conversion of $CaTiMnO_3$-based Photocatalyst for Photocatalytic Reduction of NO Via Structure-Reforming of Ti-Bearing Blast Furnace Slag. *ACS Sustainable Chemistry and Engineering*, **7**(12); 10299-10309

Zhao, H., Y. Duan, and X. Sun (2013). Synthesis and Characterization of $CaTiO_3$ Particles with Controlled shape and size. *New Journal of Chemistry*, **37**(4); 986–991

Zhou, M., J. Chen, Y. Zhang, M. Jiang, S. Xu, Q. Liang, and Z. Li (2020). Shape-Controlled Synthesis of Golf-like, Star-like, Urchin-like and Flower-like $SrTiO_3$ for Highly Efficient Photocatalytic Degradation and H2 Production. *Journal of Alloys and Compounds*, **817**; 152796

Zhuang, J., Q. Tian, S. Lin, W. Yang, L. Chen, and P. Liu (2014). Precursor Morphology-Controlled Formation of Perovskites $CaTiO_3$ and Their Photo-activity for As(III) Removal. *Applied Catalysis B: Environmental*, **156**; 108–115

Zuniga, J. P., M. Abdou, S. K. Gupta, and Y. Mao (2018). Molten-Salt Synthesis of Complex Metal Oxide Nanoparticles. *Journal of Visualized Experiments*, e58482

